

1 **The miniature paleo-speleothems record of the ‘greening’ Earth**
2 **in the early Ediacaran (635 Ma) of South China**

3 Tian Gan^{1,2,3,4}, Guanghong Zhou^{5,6*}, Shuhai Xiao^{2*}, Taiyi Luo^{1*}, Ke Pang³,
4 Mingzhong Zhou⁷, Weijun Luo⁸, Shijie Wang⁸

5 ¹ *State Key Laboratory of Ore Deposit Geochemistry, Institute of Geochemistry, Chinese Academy*
6 *of Sciences, Guiyang 550081, China*

7 ² *Department of Geosciences, Virginia Tech, Blacksburg, VA 24061, USA*

8 ³ *State Key Laboratory of Palaeobiology and Stratigraphy, Nanjing Institute of Geology and*
9 *Palaeontology and Center for Excellence in Life and Paleoenvironment, Chinese Academy of Sciences,*
10 *Nanjing, 210008*

11 ⁴ *University of Chinese Academy of Sciences, Beijing 101408, China*

12 ⁵ *School of Geography and Resources, Guizhou Education University, Guiyang 550018, China*

13 ⁶ *Guizhou Provincial Key Laboratory of Geographic State Monitoring of Watershed, Guizhou*
14 *Education University, Guiyang 550018, China*

15 ⁷ *School of Geographical and Environmental Sciences, Guizhou Normal University, Guiyang*
16 *550001, China*

17 ⁸ *State Key Laboratory of Environmental Geochemistry, Institute of Geochemistry, Chinese*
18 *Academy of Sciences, Guiyang 550081, China*

19 *E-mail address: zhouguanghong@gznc.edu.cn; xiao@vt.edu; luotaiyi@vip.gyig.ac.cn.

20 **Abstract**

21 A rapid transition from the snowball Earth to the ‘greening’ Earth in the early
22 Ediacaran, triggered by enhanced terrestrial weathering and then by elevated primary
23 productivity, has been speculated by isotope researches³. However, direct geological
24 evidence of continental weathering in the early Ediacaran is still lacking. This study
25 examines paleo-speleothems related to the karstic dissolution surface at the upmost cap
26 dolostone of the early Ediacaran Doushantuo Formation (635 Ma). Observation of
27 sheet-crack thin-sections from platform to slope facies in South China suggests that

28 plentiful speleothem-like structures in chalcedony should be interpreted as low-
29 temperature silicified calcareous paleo-speleothems. Furthermore, isopachous dolomite,
30 speleothems, chalcedony, and quartz should have filled sheet-cracks during the uplift,
31 karstification, and subsequently hydrothermal processes before the secondary
32 transgression. Thus, these widely distributed paleo-speleothems, which are direct
33 geological evidence for the 'greening' Earth in the early Ediacaran, might represent an
34 initial formation of the soil-ecosystem after the barren snowball Earth.

35 **1. Introduction**

36 Paleo-climate evolution in the Neoproterozoic (1,000-542 Ma), the most notable
37 of which was the abrupt climate transition in the aftermath of the Marinoan deglaciation
38 (~635 Ma ⁴) recorded in the 3-5 m cap dolostones and its idiosyncratic sedimentary
39 structure, was the prelude to the Cambrian explosion. Isotopic studies ¹⁻³ have described
40 a rapid evolution from a snowball Earth to a 'greening' Earth, which could greatly
41 enhance groundwater influx of photosynthetic carbon from phytomass and promote the
42 'clay mineral factory', and then subsequently increase the atmosphere's O₂ content ⁵ and
43 trigger the expansion of multicellular life. This rapid evolution centered on a drastic
44 change of the continental weathering mode which elevated the bio-available P flux and
45 promoted the marine primary productivity. Therefore, geological records of
46 contemporaneous continental weathering are important clues to understanding the
47 evolution of life in the Neoproterozoic and to illuminating the Cambrian explosion.

48 Karstification is the most important continental weathering process in carbonate
49 distribution zones, of which the environment change could be record by speleothems
50 (stalagmites, stalactites, flowstones etc.). Studies of modern karst caves suggest that
51 speleothem deposition is mostly controlled by evolution of CO₂ contents in drip-water,
52 which originate from precipitation (atmospheric CO₂) and supersaturation in soil zone
53 (CO₂ from bio-respiration and organic decomposition) and then degassing in caves ⁶⁻⁸.
54 Thus paleo-speleothems in paleo-karst, such as dripstone ⁹, micro-stalactite ^{10,11} and

55 stromatolitic laminae coatings ¹², are significant evidence for subaerial exposure and
56 paleo-pedogenesis. The widespread discontinuous karstic surface at the top of cap
57 dolostones (635 Ma) in Africa, Canada and China has disclosed a global karstic
58 dissolution event ¹³ caused by uplifting of continental shelf responding to deglacial
59 isostatic rebound ¹⁴. Hence, more detailed geological evidence such as paleo-
60 speleothems are expected to be preserved in fissures, voids and sheet-cracks related to
61 the karstic dissolution event ¹³.

62 In this paper, we report a series of miniature but delicate paleo-speleothems
63 (including stalagmites, stalactites and coatings) preserved in the sheet-crack of
64 Marinoan cap dolostone (~635 Ma) in South China. These paleo-speleothems further
65 confirm the possibility of a broad and transient continental uplift with exposure and
66 continental weathering due to the deglacial isostatic rebound.

67 **2. Geological setting and observations**

68 The Doushantuo Formation of basin, slope and platform facies is widely deposited
69 on the Yangtze Block of South China (see Fig.1 in ref. ¹³), and is underlain by Marinoan
70 deglacial tillite unit. This shows a transition from purple diamictite (<100 m) in platform
71 facies to grey diamictite (>1000 m) in basin facies. The 3-5 m cap dolostone in basal
72 Doushantuo Formation from platform to slope facies is significant with disrupted
73 massive dolomicrite and unique structures (such as giant wave ripples ¹⁵, teepee-like,
74 sheet-cracks etc. ¹⁶). A broadly karstic dissolution surface, caused by uplift by isostatic
75 rebound, has been confirmed by geological observation in South China. The total
76 duration (<1.0 Ma) from deposition to exposure and dissolution of the cap dolostone
77 has been constrained by high-precision U-Pb zircon age of 634.57 ± 0.88 Ma at the
78 topmost of Nantuo diamictite ⁴ and 635.23 ± 0.57 Ma at the topmost of cap dolostone
79 ^{17,18}, respectively. Remarkably, sheet-cracks have a uniform mineral paragenetic
80 sequence across the entire Yangtze Block: they start with isopachous dolomites
81 (sometimes with minor barite), followed by siliceous minerals (chalcedony and quartz),

82 and ending with later stage calcite and barite ¹⁹.

83 Miniature but perfect stalactites and stalagmites, which are the most typical
84 calcareous speleothems (gravitational dripping water forms) (Fig.1, Fig.2), have been
85 gradually disclosed in chalcedony cements from thick (more than 2-3 cm) sheet-cracks
86 of cap dolostones and distributing from slope (Wenghui and Daping) to platform facies
87 (Xiaofenghe and Beidoushan) sections on the Yangtze Block. Based on this discovery,
88 flat and thinner laminae, partly with botryoidal structures, that extensively encrust the
89 ceiling and floor of the sheet-cracks or breccias (Fig.3), have been interpreted here as
90 coatings (non-gravitational water-film forms).

91 **2.1 stalactite**

92 Many stalactites, hanging downwards from the ceiling of sheet-cracks and
93 exhibiting as single one or conjoined by multi-stalactites, have been found in the
94 Beidoushan and Wenghui sections (Fig. 1, 2a, 2e and 2d). The most common individual
95 stalactites are elongated columns, ranging from less than 0.4 cm to about 1.0 cm in
96 diameter, and from less than 1 cm to more than 3 cm in length.

97 Three growth stages could be identified by laminae rhythm in two vertical profiles
98 of stalactites from the Beidoushan section (Fig.1). The first is the straight soda-straw
99 with a central channel. The channel is about 100 μm in diameter and 1-2 cm in length
100 and is lined by brown organisms and filled with cryptocrystalline chalcedony. The wall
101 of the soda-straw is comprised of fibrous chalcedony with about 400-500 μm thickness
102 and it is also coated by brown organisms. The second stage is distinguished by density
103 rippling lamina couplets in flank and botryoid structures in the tip, which reflect stable
104 and slow feeding. The final stage is composed of relative broader lamina couplets which
105 reflect continuous and affluent feeding.

106 The cross-profiles of stalactites are distinguished by multilayer concentric
107 circularity structures with alternations from dark to light. The significant difference,
108 however, is the soda-straw structure, which is generally present in stalactites but
109 absolutely absent in stalagmites. The three growth stages described above can be clearly

110 observed in the cross-profiles of stalactites from the Beidoushan section. In the
111 Wenghui section, however, only two growth stages are displayed in the cross-profiles
112 of stalactites (Fig.2a, 2e and 2d) and in the vertical-profile of stalagmites. These
113 differences suggest that the two sections have different paleo-environments.

114 **2.2 stalagmite**

115 Some stalagmites, which grow upwards from the floor of the sheet-crack, were
116 discovered in Wenghui, Xiaofenghe and Beidoushan sections. They are mainly
117 composed of translucent chalcedony, which makes them obviously distinguished from
118 the surrounding white crystalline quartz in hand-specimens of the Wenghui and
119 Beidoushan sections (Fig.2b, 2d and 2f). Most of them are cylindric in shape, slightly
120 wider in the root and narrower in the tip, with length concentrated around 1-3.5 cm and
121 diameters of about 0.5-1.3 cm. This thin diameter style, classified as "Minimum-
122 diameter" stalagmite²⁰, is coincident with the short drip fall height²¹ in the sheet-cracks.

123 A perfect vertical profile of stalagmite from the Wenghui section shows a clear
124 transition of growth style (Fig.2b) under a reflecting light microscope, while, such a
125 transition is relatively blurred under transmitted light. The early growth style is
126 distinguished by a stacked botryoid structure, which could be observed in the bottom
127 part of modern stalagmites²²⁻²⁵ (Fig.2b) and which represent turbulence of the dripping
128 water at the beginning of stalagmite deposition or indigent feeding and slow
129 precipitation²⁶. The later growth is significant with continuous and smooth rhythmical
130 laminae couplets by a dark and a light lamina, which is similar to modern calcareous
131 stalagmites^{25,27,28} and which represent affluent feeding and stable precipitation^{22,29-31}.
132 The rhythmical laminae are about 350 μm thick and contain about 20-30 lamina
133 couplets.

134 There is one complete stalagmite and three complete stalactite cross-profiles in the
135 same slide, the latter of which are characterized by a central channel texture (Fig.2d).
136 There are two growth stages. The first of these is typical of unity cryptocrystalline
137 chalcedony and the latter of them is features concentric fibrous chalcedony laminae,

138 corresponding to the two-growth style in the vertical profile as mentioned above
139 (Fig.2b). There are about 20-30 laminae couplets within the 2100 μm thick outer zone
140 and this is rich in organics as seen by the obvious increase in fluorescence (Fig.2c, 2e
141 and 2f) when compared to the inner zone. Significantly, residue calcite core and laminae
142 have been observed in one stalagmite cross-profile from the Xiaofenghe section
143 (Fig.3h).

144 **2.3 coatings**

145 In almost all of the cap dolostone sections in South China, the wall (mainly
146 composed of ceiling and floor) of the sheet-cracks and the breccias in them are
147 extensively covered with less than 0.1 cm to 1 cm thick chalcedony coatings, which
148 tend to have fairly continuous layers, and are characterized by visible rippled growth
149 morphology and stacked layering (Fig. 3). Remarkably, partly silicified calcite coatings,
150 which could be distinguished under reflected light and scanning electron microscope
151 (SEM) (Fig.3e and 3f), was preserved in the Daping section. The coatings may be
152 botryoidal (Fig. 3b), or even spiral (looks like vermiform helictites) (Fig.3c and 3d),
153 but in most cases they are smoothly curving along the wall of the sheet-crack and the
154 breccias with stable thickness (Fig. 3a). On the whole, the coatings comprise of 15-30
155 lamina couplets, which are much more obvious in ultraviolet fluorescent (Fig.2c and
156 3g), with single couplet thickness ranging from 20 μm to 60 μm . These morphology
157 and laminae structure indicate that the smooth coatings periodically precipitated from
158 adhesive water-films condensed from humid caves, the botryoidal structure are
159 produced by surface tension dividing water-films into drops and the vermiform
160 helictites produced by the addition of drip water to already present water-films.

161 **3. Discussion**

162 Protogenetic siliceous speleothems are commonly developed in caves or lava
163 tunnels overlain by silicate rocks (such as quartzites, sandstones, granites etc.)³².
164 Although platform-wide black shale overlaid on the cap dolostone³³ seems to be a

165 potential silica source, lack of karstic surface and weathering dissolution textures in the
166 black shale suggests that the sheet-crack speleothems were not protogenetic siliceous
167 speleothems and were constrained before the deposition of the black shale. Indeed, the
168 sheet-crack speleothems are confined below the widespread paleo-karstic surface the
169 age of which has been previously determined by two ash beds with zircon U-Pb age of
170 634.57 ± 0.88 Ma and 635.23 ± 0.57 Ma^{17,18} respectively. Additionally, the coatings in
171 the Daping section are mostly consisted of calcareous laminae (Fig. 3e and 3f) and the
172 silicified stalactites in Xiaofenghe section still retain a few calcareous laminae (Fig. 3h).
173 Therefore, the sheet-crack speleothems deposited at ca. 635Ma were originally
174 calcareous speleothems, which is akin to modern silicification-preserved speleothems
175 formed by low-temperature metasomatism of primary calcareous speleothems^{34,35}.

176 Three successive events associated with the Marinoan cap dolostone in South
177 China have been summarized as such¹³: (1) the first postglacial transgression and
178 deposition of the cap dolostone; (2) isostatic rebound, uplift and karstification of the
179 cap dolostone; and (3) the second postglacial transgression, multiphase cave fillings
180 and post-cap deposition. Multiple mineral generations on walls of sheet-cracks are
181 attributed to the beginning of the second postglacial transgression¹³ or a low-
182 temperature hydrothermal episode^{19,36}, however, minerals corresponding to the uplift
183 and karstification event have not been depicted. No obvious dissolution phenomena by
184 later erosion have been observed on the surface of the paleo-speleothems, indicating
185 that the deposition of the paleo-speleothems has been quickly terminated by the low
186 temperature hydrothermal process. Given that the hydrothermal episode developed
187 after the beginning of the second transgression, chert lens (as siliceous tufa) should be
188 observed upon the karstic surface, nevertheless, siliceous cements and veins have been
189 strictly confined beneath the karstic surface. Thus we interpret the deposition and
190 hydrothermal silicification of the sheet-crack calcareous speleothems as successive
191 processes during exposure and karstification.

192 Modern karst studies indicate that necessary condition for karstic dissolution is the

193 soil-ecosystem (soil, plant, microbial, etc.), which afford organic matter and plentiful
194 CO₂^{37,38} in the water of an epikarst zone and hence the relative speleothems could
195 partly record the overlying ecosystem information. Karst dissolution in some high-
196 altitude and cold-climate regions occurs in the absence of soil⁷, however, and so
197 obviously a temperature gradient caused by a huge altitude drop is needed to form
198 speleothems in these conditions. Paleo-karsts are defined as karsts developed largely or
199 entirely during past geological periods³⁹. Freytet (2002) refers to karsts or vugs that
200 are centimeters to decimeters as microkarsts¹¹, and these are an important evidence of
201 ancient subaerial exposure and paleosols formation^{9,11,40}. Like pseudomicrokarsts¹¹,
202 we define the microkarsts developed in past geological periods as paleomicrokarsts, in
203 which the speleothems are defined as paleomicrospeleothems. The Precambrian
204 palaeosols are habitats for early terrestrial life. The paleomicrospeleothems in the
205 corresponding carbonate strata are important geological evidence that record the early
206 biological evolution of the Earth. Paleomicrospeleothems (fibrous flowstone lining
207 grike system) found in the Mesoproterozoic in Canada⁴¹ and U.S.A³⁵ and the exquisite
208 paleomicrospeleothems (icicle-like pendants, hemispherical protrusions and ground-up
209 columns) reported in the Dengying Formation⁴² may represent contemporaneous
210 pedogenesis processes. In the early Ediacaran, although recovery of ocean-ecosystem
211 from the brutal snowball Earth had been confirmed by vase-shaped fossils in tillite, the
212 geological evidence for terrestrial-ecosystem revival are still expected yet. Here, the
213 silicified paleomicrospeleothems preserved in the 3-5 m cap dolostone suggest that the
214 soil-ecosystem had been broadly established in South China just after uplifting and
215 exposing of the cap dolostone.

216 **4. Summary and Implication**

217 This paper reports the widely distributed miniature silicified paleospeleothems in
218 sheet-cracks in Marinoan cap dolostone from South China, which depict specific karstic
219 process of the cap dolostone during uplifting and exposure caused by isostatic rebound.

220 These are 1) miniature speleothem growth during karstification; 2) speleothem
221 termination and silicification by low-temperature fluid before the second transgression.
222 These paleo-speleothems have recorded the rapid recovery of the soil-ecosystem after
223 a snowball Earth during cap dolostone rebound and karstic dissolution, which is key
224 geological evidence for the 'green' Earth model.

225 The karstic dissolution surface may have been widely distributed on a global scale
226 at early Ediacaran, implying that the coincident silicified calcareous paleo-speleothems
227 are also global distributed. The silicification preservation process has destroyed some
228 original geochemical information such as carbon/oxygen isotopes, but the plentiful
229 organic-rich laminae are preserved. Thus, the bio-markers in these organic-rich laminae
230 are expected to further document the evolution of soil-ecosystem.

231 **Acknowledgements**

232 This research was supported by the National Nature Science Fund of China
233 (41802027, 41873058), Natural Science and Technology Fund of Guizhou Province,
234 China [JZ(2015)2009], and the incentive subsidy funds from the Guizhou Education
235 University in 2019 for projects of the Ministry of Science and Technology and the
236 National Natural Science Fund of China: Study on paleo-karst structure preserved in
237 cap dolostone of Doushantuo Formation in South China. T.G. acknowledges financial
238 support from China Scholarship Council. We thank Chuanming Zhou for helpful
239 discussions and Joshua Musir for English correction.

240 **Author Contributions**

241 T.L., G.Z., and T.G. designed the research. T.L., G.Z., and T.G. collected the
242 samples. G.Z and T.G. conducted experiments. G.Z., T.L., S.X., and T.G. developed the
243 interpretation and prepared the manuscript with contributions from K.P, M.Z, W.L and
244 S.W.

245 **Methods**

246 Three sheet-crack samples (14XFH-1, 14XFH-3 and 14XFH-5) from Xiaofenghe
247 section (N30°48'54", E111°03'20"), Hubei Provinces, three sheet-crack samples
248 (14DPc1-1, 14DPc1-2 and 14DPc1-3) from Daping section (N28°59'01", E110°27'42"),
249 Hunan Provinces, four sheet-crack samples (16WH-1, 16WH-2, 16WH-3 and 16WH-
250 4) from Wenghui section (N27°49'55", E109°01'32") , Guizhou Provinces and four
251 samples (18BDS-2, 18BDS-4, 18BDS-7 and 18BDS-9) from Beidoushan section
252 (N27°01'40", E107°23'22"), Guizhou Provinces were collected from the cap dolostone
253 of the Doushantuo Formation in South China. Petrographic slices (100 µm and 200 µm
254 in thickness) and polished slabs of the sheet-crack samples were cut both perpendicular
255 and horizontal to bedding plane and investigated under transmitted light microscopy
256 (TLM), reflected light microscopy (RLM) and fluorescent light microscopy (FLM).

257

258 **Reference**

- 259 1 Kennedy, M., Droser, M., Mayer, L. M., Pevear, D. & Mrofka, D. Late Precambrian
260 oxygenation; inception of the clay mineral factory. *Science* **311**, 1446-1449 (2006).
- 261 2 Knauth, L. P. & Kennedy, M. J. The late Precambrian greening of the Earth. *Nature* **460**, 728
262 (2009).
- 263 3 Kump, L. R. Hypothesized link between Neoproterozoic greening of the land surface and the
264 establishment of an oxygen-rich atmosphere. *Proceedings of the National Academy of Sciences* **111**,
265 14062-14065 (2014).
- 266 4 Condon, D. *et al.* U-Pb ages from the neoproterozoic Doushantuo Formation, China. *Science*
267 **308**, 95-98, doi:10.1126/science.1107765 (2005).
- 268 5 Zhou, C., Yuan, X., Xiao, S., Chen, Z. & Hua, H. Ediacaran integrative stratigraphy and
269 timescale of China. *Science China Earth Sciences* **62**, 7-24, doi:10.1007/s11430-017-9216-2 (2019).
- 270 6 Baker, A., Barnes, W. L. & Smart, P. L. Speleothem luminescence intensity and spectral
271 characteristics: Signal calibration and a record of palaeovegetation change. *Chemical Geology* **130**, 65-
272 76, doi:https://doi.org/10.1016/0009-2541(96)00003-4 (1996).
- 273 7 Frisia, S. & Borsato, A. in *Developments in Sedimentology* Vol. 61 (eds A. M. Alonso-Zarza
274 & L. H. Tanner) 269-318 (Elsevier, 2010).
- 275 8 Dorr, H. & Munnich, K. O. Annual Variations of the 14C Content of Soil CO₂. *Radiocarbon*
276 **28**, 338-345 (1986).
- 277 9 Amodio, S., Barattolo, F. & Riding, R. Early Cretaceous dendritic shrub-like fabric in

- 278 karstified peritidal carbonates from southern Italy. *Sedimentary Geology* **373**, 134-146,
279 doi:10.1016/j.sedgeo.2018.06.001 (2018).
- 280 10 Qing, H. & Nimegeers, A. R. Lithofacies and depositional history of Midale carbonate-
281 evaporite cycles in a Mississippian ramp setting, Steelman-Bienfait area, southeastern Saskatchewan,
282 Canada. *Bulletin of Canadian Petroleum Geology* **56**, 209-234, doi:10.2113/gscpgbull.56.3.209 (2008).
- 283 11 Freytet, P. & Verrecchia, E. P. Lacustrine and palustrine carbonate petrography: an overview.
284 *Journal of Paleolimnology* **27**, 221-237, doi:10.1023/a:1014263722766 (2002).
- 285 12 Alvaro, J. J. & Clausen, S. Microbial crusts as indicators of stratigraphic diastems in the
286 Cambrian Breche a Micmacca, Atlas Mountains of Morocco. *Sedimentary Geology* **185**, 255-265,
287 doi:10.1016/j.sedgeo.2005.12.025 (2006).
- 288 13 Zhou, C., Bao, H., Peng, Y. & Yuan, X. Timing the deposition of 17O-depleted barite at the
289 aftermath of Nantuo glacial meltdown in South China. *Geology* **38**, 903-906 (2010).
- 290 14 Hoffman, P. F. & Macdonald, F. A. Sheet-crack cements and early regression in Marinoan
291 (635 Ma) cap dolostones: Regional benchmarks of vanishing ice-sheets? *Earth and Planetary Science*
292 *Letters* **300**, 374-384, doi:10.1016/j.epsl.2010.10.027 (2010).
- 293 15 Allen, P. A. & Hoffman, P. F. Extreme winds and waves in the aftermath of a Neoproterozoic
294 glaciation. *Nature* **433**, 123, doi:10.1038/nature03176 (2005).
- 295 16 Jiang, G., Kennedy, M. J., Christie-Blick, N., Wu, H. & Zhang, S. Stratigraphy, sedimentary
296 structures, and textures of the late Neoproterozoic Doushantuo cap carbonate in South China. *Journal of*
297 *Sedimentary Research* **76**, 978-995 (2006).
- 298 17 Zhou, C., Lang, X., Huyskens, M. H., Yin, Q.-Z. & Xiao, S. Calibrating the terminations of
299 Cryogenian global glaciations. *Geology* **47**, 251-254, doi:10.1130/g45719.1 (2019).
- 300 18 Condon, D. *et al.* U-Pb Ages from the Neoproterozoic Doushantuo Formation, China. *Science*
301 **308**, 95-98 (2005).
- 302 19 Zhou, G., Luo, T., Zhou, M., Xing, L. & Gan, T. A ubiquitous hydrothermal episode recorded
303 in the sheet-crack cements of a Marinoan cap dolostone of South China: Implication for the origin of the
304 extremely C-13-depleted calcite cement. *Journal of Asian Earth Sciences* **134**, 63-71,
305 doi:10.1016/j.jseaes.2016.11.007 (2017).
- 306 20 Fairchild, I. J. & Baker, A. *Speleothem science: from process to past environments*. Vol. 3
307 (John Wiley & Sons, 2012).
- 308 21 Gams, I. Contribution to morphometrics of stalagmite. *Proceedings of the 8th International*
309 *Congress of Speleology* **8**, 276-278 (1981).
- 310 22 Tan, M. *et al.* Applications of stalagmite laminae to paleoclimate reconstructions: Comparison
311 with dendrochronology/climatology. *Quaternary Science Reviews* **25**, 2103-2117,
312 doi:https://doi.org/10.1016/j.quascirev.2006.01.034 (2006).
- 313 23 Baker, A., Smart, P. L., Edwards, R. L. & Richards, D. A. ANNUAL GROWTH BANDING
314 IN A CAVE STALAGMITE. *Nature* **364**, 518-520, doi:10.1038/364518a0 (1993).
- 315 24 Tan, L. *et al.* Quantitative temperature reconstruction based on growth rate of annually-layered
316 stalagmite: a case study from central China. *Quaternary Science Reviews* **72**, 137-145,
317 doi:10.1016/j.quascirev.2013.04.022 (2013).
- 318 25 Railsback, L. B. *et al.* The timing, two-pulsed nature, and variable climatic expression of the
319 4.2 ka event: A review and new high-resolution stalagmite data from Namibia. *Quaternary Science*

- 320 *Reviews* **186**, 78-90, doi:<https://doi.org/10.1016/j.quascirev.2018.02.015> (2018).
- 321 26 Dreybrodt, W. & Romanov, D. REGULAR STALAGMITES: THE THEORY BEHIND
322 THEIR SHAPE. *Acta Carsologica* **37**, 175-184 (2008).
- 323 27 Tan, L. *et al.* Quantitative temperature reconstruction based on growth rate of annually-layered
324 stalagmite: A case study from central China. *Quaternary Science Reviews* **72**, 137-145 (2013).
- 325 28 Baker, A., Smart, P. L., Edwards, R. L. & Richards, D. A. Annual growth banding in a cave
326 stalagmite. *Nature* **364**, 518-520 (1993).
- 327 29 Baker, A., Proctor, C. J. & Barnes, W. L. Stalagmite lamina doublets: a 1000 year record of
328 extreme winters in NW Scotland. *International Journal of Climatology* **22** (2002).
- 329 30 Wang, X. *et al.* PRELIMINARY ANALYSES BY SIMS ON TRACE COMPONENTS OF
330 STALAGMITE MICROLAYERS AND THEIR CLIMATE SIGNIFICANCE. *Quaternary Science Reviews* **19**, 59-
331 66,97-98 (1999).
- 332 31 Brook, G. A., Rafter, M. A., Railsback, L. B., Sheen, S. W. & Lundberg, J. A high-resolution
333 proxy record of rainfall and ENSO since AD 1550 from layering in stalagmites from Anjohibe Cave,
334 Madagascar. *Holocene* **9**, 695-705, doi:10.1191/095968399677907790 (1999).
- 335 32 Aubrecht, R., Brewercarias, C., Smida, B., Audy, M. & Kovacik, L. Anatomy of biologically
336 mediated opal speleothems in the World's largest sandstone cave: Cueva Charles Brewer, Chimantá
337 Plateau, Venezuela. *Sedimentary Geology* **203**, 181-195 (2008).
- 338 33 R. C., T. T. & Y, X. *Research on Sinian Strata with ore deposits in the Yangzi (Yangtze) region,*
339 *China.* (1989).
- 340 34 Wheeler, W. H. & Textoris, D. A. Triassic Limestone and Chert of Playa Origin in North
341 Carolina. *Journal of Sedimentary Research* **48**, 765-776 (1978).
- 342 35 Skotnicki, S. J. & Knauth, L. P. The Middle Proterozoic Mescal Paleokarst, Central Arizona,
343 U.S.A.: Karst Development, Silicification, and Cave Deposits. *Journal of Sedimentary Research* **77**,
344 1046-1062 (2007).
- 345 36 Cui, Y. *et al.* Germanium/silica ratio and rare earth element composition of silica-filling in
346 sheet cracks of the Doushantuo cap carbonates, South China: Constraining hydrothermal activity during
347 the Marinoan snowball Earth glaciation. *Precambrian Research*, 105407,
348 doi:<https://doi.org/10.1016/j.precamres.2019.105407> (2019).
- 349 37 Blyth, A. J. *et al.* Molecular organic matter in speleothems and its potential as an
350 environmental proxy. *Quaternary Science Reviews* **27**, 905-921 (2008).
- 351 38 Kaufmann, G. Stalagmite growth and palaeo-climate: the numerical perspective. *Earth and*
352 *Planetary Science Letters* **214**, 251-266 (2003).
- 353 39 Bosak, P., Ford, D. C., Glazek, J. & Horacek, I. (Academia, Publishing House of the
354 Czechoslovak Academy of Sciences, Prague, Czechoslovakia, 1989).
- 355 40 Semeniuk, V., Percival, I. G. & Brocx, M. Subaerial disconformities, microkarst and paleosols
356 in Ordovician limestones at Bowan Park and Cliefden Caves, New South Wales, and their geoheritage
357 significance. *Australian Journal of Earth Sciences* **66**, 891-906, doi:10.1080/08120099.2019.1577297
358 (2019).
- 359 41 Kerans, C. & Donaldson, J. A. *Proterozoic Paleokarst Profile, Dismal Lakes Group, N.W.T.,*
360 *Canada 1.* (1988).
- 361 42 Ding, Y. *et al.* Cavity-filling dolomite speleothems and submarine cements in the Ediacaran

362 Dengying microbialites, South China: Responses to high-frequency sea-level fluctuations in an
363 'aragonite-dolomite sea'. *Sedimentology*, doi:10.1111/sed.12605 (2019).

364 **Figure Legends**

365 **Figure 1 | Polished slab and micrographs of stalactite from Beidoushan**
366 **section. a**, Polished slab shows stalactites in a sheet-crack scanning by a HP ScanJet,
367 the white solid rectangle highlights a column (connective bodies of stalactite and
368 stalagmite), white dotted rectangles highlight conjunction stalactites, the yellow arrow
369 denotes a single complete stalactite with “soda straw” drip channel. **b**, Petrographic slice
370 shows transverse and vertical sections of stalactite under TLM (transmission light
371 microscope), the white and red arrows denote the vertical and transverse sections of
372 “soda straw” drip channel, respectively. **c**, Enlarged view of the stalactite vertical
373 section in **b** (rectangle) under FLM (fluorescent light microscope), the white arrow
374 denotes the vertical section of “soda straw” drip channel. **d**, Enlarged view of stalactite
375 transverse in **b** (rectangle) under FLM, red arrows denote the transverse of “soda straw”
376 drip channel.

377

378 **Figure 2 | Polished slabs and micrographs of stalagmite, stalactite and coating**
379 **from Wenghui section. a**, Polished slab showing stalagmite, stalactite and coating in a
380 sheet-crack, white dotted lines highlight the coating areas in the sheet-crack, white
381 arrows denote stalactites, yellow arrows denote stalagmites. **b**, Petrographic slice shows
382 a vertical section of stalagmite and coating under RLM, white dotted lines highlight the
383 coating areas. **c**, Enlarged view of coating vertical section shows the organic-rich
384 laminae in **b** (rectangle) under FLM. **d**, Petrographic slice shows stalagmite and
385 stalactite transverses under TLM, red arrows and yellow arrows denote a single “soda
386 straw” drip channel and the aggregation of “soda straw” drip channel, respectively. **e**,
387 Enlarged view of a stalactite vertical section in **d** (rectangle) under FLM, showing the
388 organic-rich laminae and “soda straw” drip channel. **f**, Enlarged view of a stalagmite
389 transverse section in **d** (rectangle) under FLM, showing the organic laminae but lack of

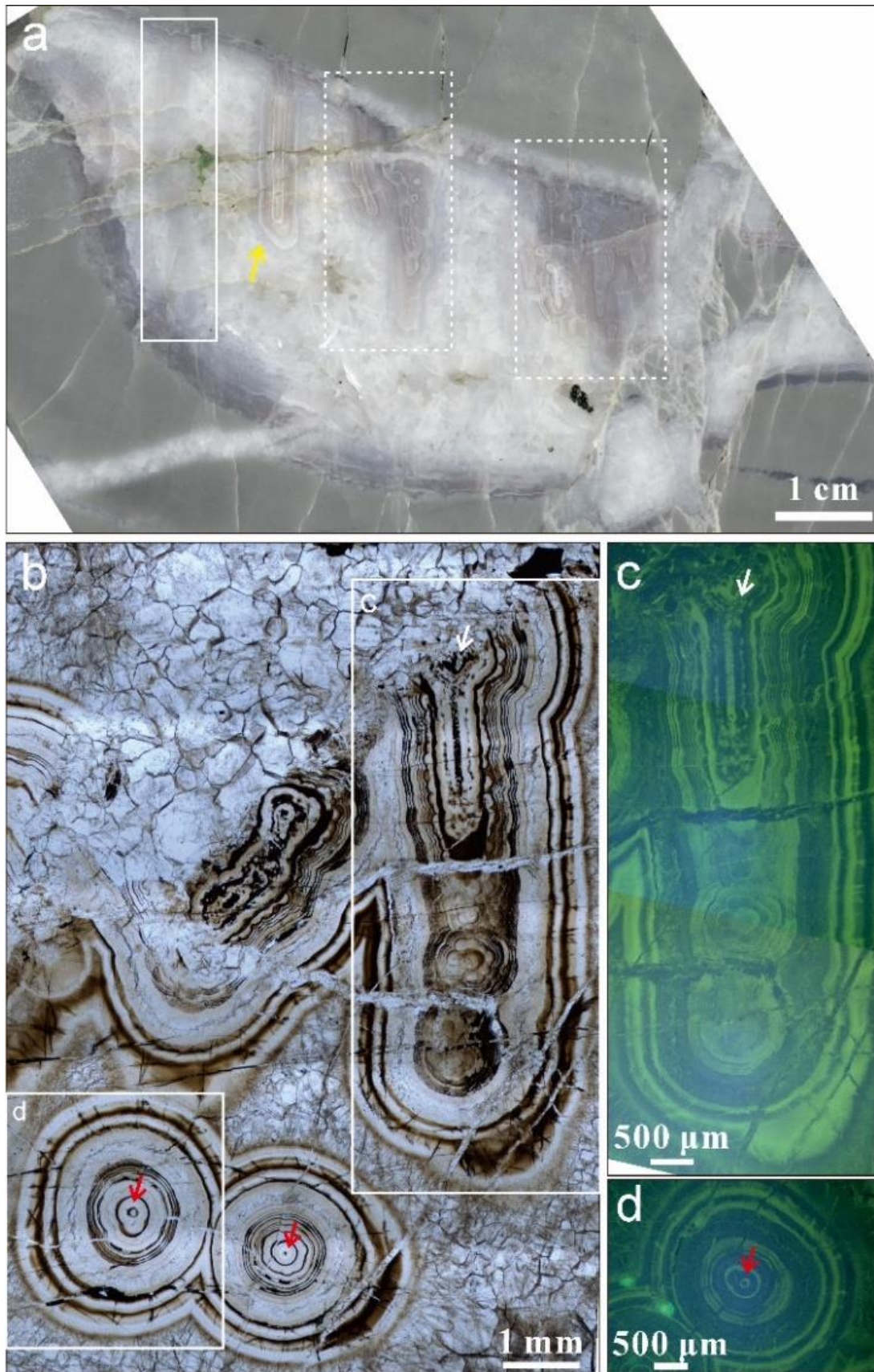
390 “soda straw” drip channel.

391

392 **Figure 3 | Polished slab, hand specimen and micrographs of coatings and a**
393 **special stalactite. a**, Polished slab shows coatings in a sheet-crack, white arrows denote
394 the coating of a dolostone breccia. **b**, Hand specimen shows a coating lining in a sheet-
395 crack, white dotted line highlights the coating boundary, black and red arrow denote
396 botryoidal and mold structure of the coating. **c**, Petrographic slice shows a coating with
397 a vermiform-like helictite under FLM. **d**, Enlarged view of the helictite in **c** (rectangle)
398 under SEM (scanning electron microscope). **e**, Petrographic slice shows a partly
399 silicified organic-rich calcareous coating under TLM. **f**, Enlarged view of the coating
400 in **e** (rectangle) under SEM, showing the silicified calcareous coating, white arrows
401 highlight the siliceous cements. **g**, Enlarged view of the coating in **e** (rectangle) under
402 FLM, showing the organic-rich laminae. **h**, Petrographic slice shows a silicified
403 stalactite under TLM, white arrows highlight the residual calcite laminae. **a, c and d**
404 from Beidoushan section, **b** from Zhangcunping section, **e-g** from Daping section, **h**
405 from Xiaofenghe section.
406

407

Fig. 1

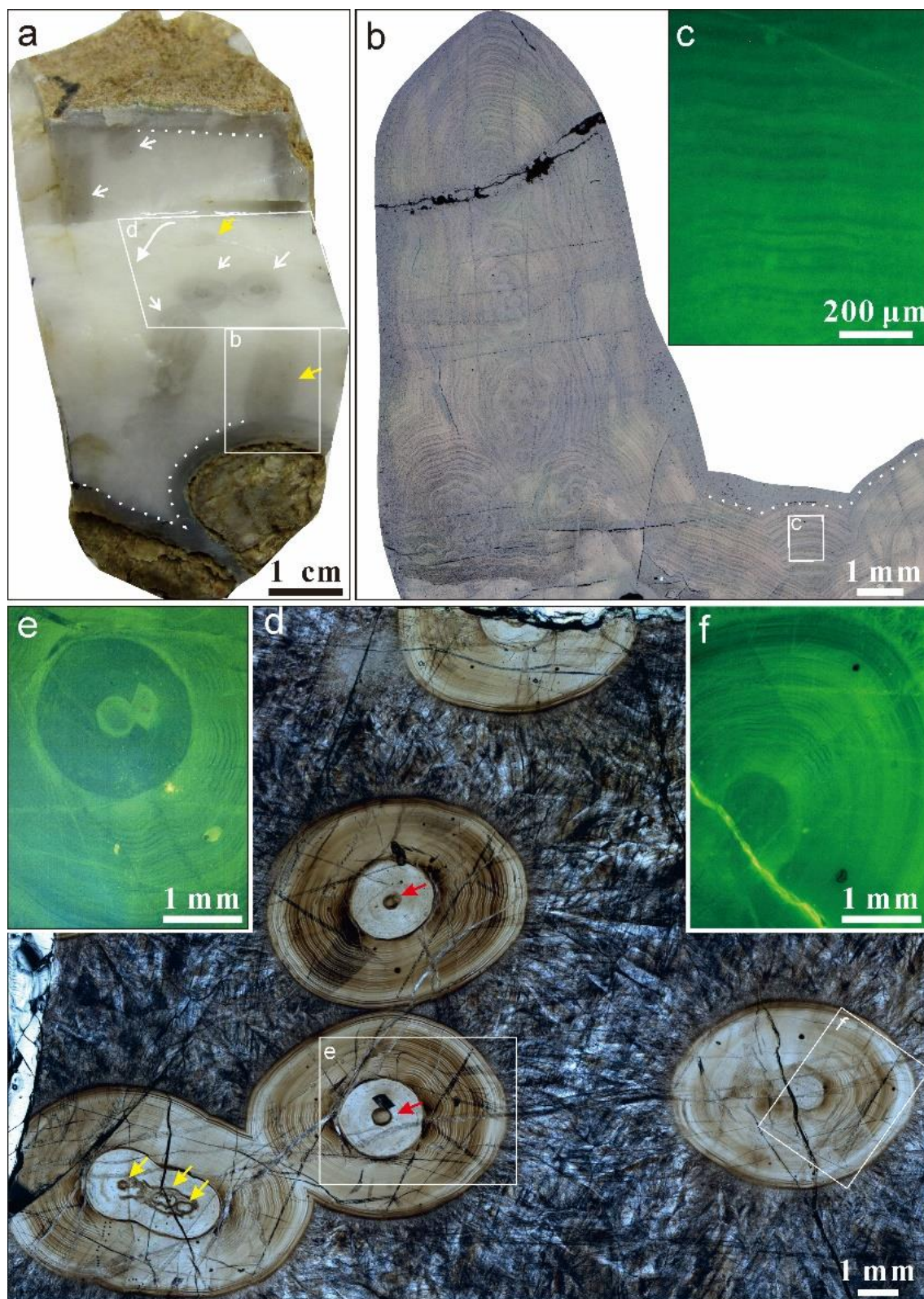


408

409

410

Fig. 2

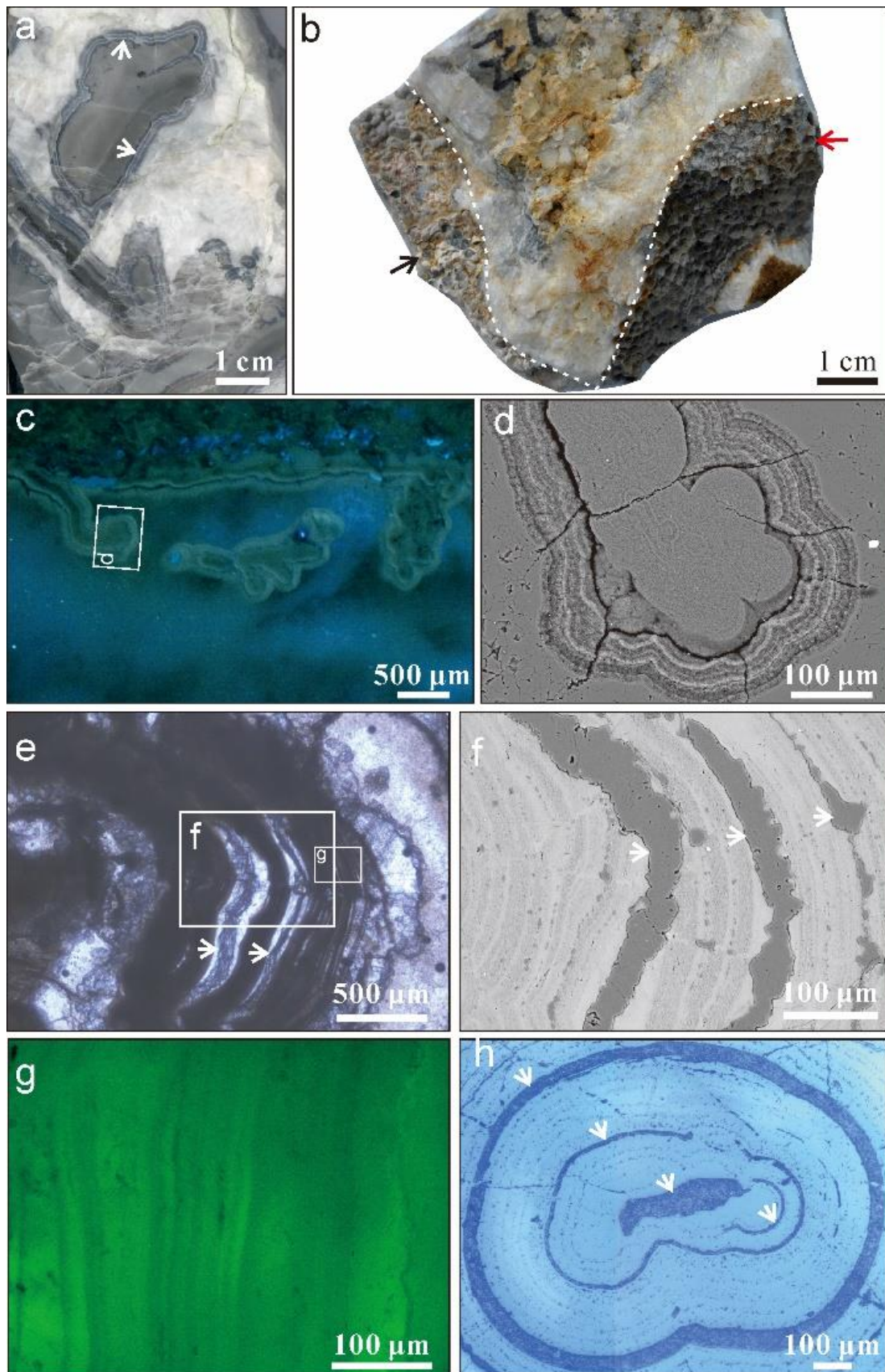


411

412

413

Fig. 3



414